Egyptian Journal of Chemistry

http://ejchem.journals.ekb.eg/

New Eco-Friendly Surfactant Corrosion Inhibitors Derived from Polyethylene Glycol: Surface Activity, Gravimetric, Electrochemical, Theoretical Quantum Computation, and Simulation Analysis

Madiha M Hegazy,[1] Eid M. Khalil,[1] Mahmoud A.F Mansour,[2,*],Emad Badr,[3]

[1] Department of Chemistry, Faculty of Science, Helwan University, Ain Helwan, Cairo 11795, Egypt
[2] Corrosion Resistance Department, General Petroleum Company, Red sea,Ras gharib 84727, Egypt, ma.abosehly@gmail.com
[3] Egyptian Petroleum Research Institute (EPRI), Nasr City, Cairo 11727, Egypt

Abstract

Corrosion inhibitors are vital for infrastructure preservation from corrosion, cost savings, and environmental protection. Recognizing ecological consequences underscores the need for eco-friendly inhibitor development and proactive management to safeguard resources and ecosystems. In this study, Development of eco-friendly Gemini surfactants based on PEG derivatives, systematically varying PEG molecular weight, characterized by FTIR and 1H NMR, with detailed corrosion inhibition evaluation and computational studies. PEG derivative surfactants were synthesized from different molecular weights (400, 1000, 4000, 6000) of PEG via oxidation with chromic acid. The resulting PEG carboxylic acid intermediates were then amidated with N, N-Dimethylpropane-1,3-diamine and converted into cationic Gemini surfactant bromide compounds using 1-Bromooctane. In 1 N HCl, surface activity was measured at 25°C, 40°C, and 60°C, showing that as temperature increases, surface tension decreases, and CMC values rise for all synthesized surfactants. PE-Br-6000 exhibited higher corrosion inhibition efficacy (%ηw) at 400 ppm (95.5%, 97.5%, 98.0%) compared to PE-Br-4000 (92.6%, 94.9%, 95.1%), PE-Br-1000 (90.0%, 92.0%, 93.2%), and PE-Br-400 (87.4%, 87.6%, 90.8%) at 25°C, 55°C, and 70°C. Potentiodynamic polarization showed PE-Br-6000's efficacy at 25°C was 89.3%, surpassing PE-Br-4000 (85.9%), PE-Br-1000 (85.2%), and PE-Br-400 (84.8%). Electrochemical impedance spectroscopy indicated PE-Br-6000's 95.6% efficacy at 25°C, outperforming PE-Br-4000 (95.3%), PE-Br-1000 (95.2%), and PE-Br-400 (95.0%). Quantum computational studies used Gaussian 09W (RHF theory, Sto-3G basis sets) and Monte Carlo (MC) Simulation with Biovia Material Studio software (2020). Further PEG derivative research involves exploring wider molecular weight ranges and structural modifications. Enhanced synthesis, extended corrosion testing, computational modeling, and environmental assessments aim to optimize eco-friendly corrosion inhibitors for improved infrastructure protection.

Keywords: PEG derivatives surfactants, Eco-friendly, Gemini surfactant, Corrosion inhibitors, surface activity, and computational analysis.

1. Introduction

Surfactants, or surface agents, are vital in many industries, especially oil and gas. They reduce surface tension between solids and liquids, preventing gas hydrate formation, optimizing drilling efficiency, maximizing oil recovery, and protecting pipelines from corrosion. In enhanced oil recovery (EOR) [1].surfactants lower the tension between oil and water, aiding in oil extraction from reservoir rocks. Drilling fluids with surfactants improve lubrication and reduce friction, minimizing drill bit wear and ensuring operational stability[2]. Polymeric surfactants are highly valuable due to their unique properties. Their larger size provides greater stability and less migration or evaporation. They also have improved solubility in both polar and nonpolar solvents due to their amphiphilic nature. Compared to small-molecule surfactants, polymeric surfactants offer synthetic advantages, making them useful in many industries.[3]. Reducing environmental impact during the development of new cleaning agents is crucial due to stricter environmental regulations. [4]. Increased biodegradability is achieved by adding cleavable groups between the hydrophilic and hydrophobic parts of surfactants. These groups, including amide, ethoxylate, and ester, are easily hydrolysed and break down into basic components. Biodegradable surfactants are essential because they readily biodegrade in various environments.[5]–[8]. The use of eco-friendly polyethylene glycol amide surfactant derivatives as corrosion inhibitors has grown recently. Understanding their behaviour at various concentrations is crucial for effective formulation. As surfactant concentrations in water increase, surface concentration rises until the critical micelle concentration (CMC) is reached. Determining the CMC, often done with tensiometers, is vital for effective formulations. Acid additions, like hydrochloric acid (HCl), can reduce surface tension significantly, enhancing gas well stimulation and demonstrating the effectiveness of these surfactants. Gemini surfactants, with two hydrophilic heads and two hydrophobic tails, have lower

*Corresponding author e-mail: ma.abosehly@gmail.com.; (Mahmoud A.F Mansour).
Receive Date: 10 March 2024, Revise Date: 04 June 2024, Accept Date: 01 July 2024
DOI: 10.21608/ejchem.2024.274647.9412

CMCs and reduce surface tension more effectively than monomeric surfactants. Their ability to form various structures makes them valuable for applications like emulsification, coating, dispersion, and corrosion inhibition.[9], [10] The development of eco-friendly Gemini surfactants based on PEG derivatives is the focal point of this study, which aims to synthesize and evaluate the corrosion inhibition properties of these novel compounds. This research addresses the pressing need for environmentally benign alternatives to conventional corrosion inhibitors. By systematically varying the molecular weights of PEG (400, 1000, 4000, and 6000), the study investigates the relationship between molecular structure and inhibition efficacy. This systematic approach enables a detailed understanding of how PEG molecular weight impacts the performance of the Gemini surfactants. Comprehensive characterization of the synthesized surfactants was conducted using Fourier-transform infrared (FTIR) and proton nuclear magnetic resonance (1H NMR) spectroscopy. Additionally, their surface activity and corrosion inhibition efficacy were thoroughly evaluated through weight loss measurements, potentiodynamic polarization, and electrochemical impedance spectroscopy across different temperatures. To further elucidate the mechanisms at play, Gaussian 09W and Monte Carlo simulations were employed, offering molecular-level insights into the interactions between the surfactants and metal surfaces. The novelty of this work lies in the synthesis, characterization, and extensive evaluation of a new class of eco-friendly Gemini surfactants derived from PEG, with a particular focus on understanding the impact of PEG molecular weight on corrosion inhibition efficiency.

2. Empirical research methods

2.1. Chemical substances and synthesis processes.

N, N-Dimethylpropane-1,3-diamine, and Ether were acquired from Alfa Aesar, while Octanoyl bromide, Potassium dichromate, 98% sulfuric acid, Chloroform (CHCl3), Magnesium sulphate (MgSO4), and Sodium Chloride (NaCl) were obtained from Sigma-Aldrich. Various polyethylene glycols (PEG) with distinct molecular weights (specifically PEG-400, PEG-100, PEG-4000, and PEG-6,000) were sourced from Merck. The surfactants PE-Br-400, PE-Br-1000, PE-Br-4000, and PE-Br-6000 employed in this study were prepared following a specific synthesis procedure. To commence, the initial step involves the preparation of chromic acid. This procedure entails the gradual addition of an aqueous solution, specifically 0.235 grams of potassium dichromate (K2CrO3), dissolved in 5 milliliters of water, to a solution consisting of 25 milliliters of water along with 8 milliliters of concentrated sulfuric acid (98%). This addition is performed incrementally and under continuous string for a duration spanning 4 to 5 hours, ultimately leading to the formation of chromium trioxide.

Next, add 25ml of water containing 5g of PEG 400-6000 to the chromium trioxide solution and stir until it turns a green-blue color. Extract the solution with 3 X CHCl3 (100ml). blend the organic layers and rinse them with water (2 X 25ml) and a saturated NaCl solution (2 X 25ml) using a separation funnel. After combining the organic layers again, dry them with MgSO4. Concentrate the mixture under reduced pressure and precipitate the PEG-carboxylate by adding 150ml of ether. Filter and dry the solid PEG-carboxylic acid (4.9g, 96% yield).[11]

0.1 moles of PEG-carboxylic acid underwent a reaction with 0.2 moles of N1, N3-Dimethylpropane-1,3-diamine with using xylene as the solvent. This reaction was conducted under heating at 100°C for a duration of 24 hours, during which 0.2 moles of water were liberated. This resulted in the formation of PEG-bis(N1,N3-Dimethylpropane-1,3-diamine) carboxylate. The solvent was then removed using vacuum evaporation. The obtained product was then subjected to a reaction with 1-Bromooctane to yield a compound denoted as 2,2'-(poly(ethane-1,2-diylbis(oxy))bis(N-(3-(methylamino)propyl)-N-ethyl-N-octyl acetamide) bromide. This reaction took place with using ethanol as the solvent and was heated at 100°C for a duration of 100 hours. The schematic representation of this reaction scheme is illustrated in Fig.1.

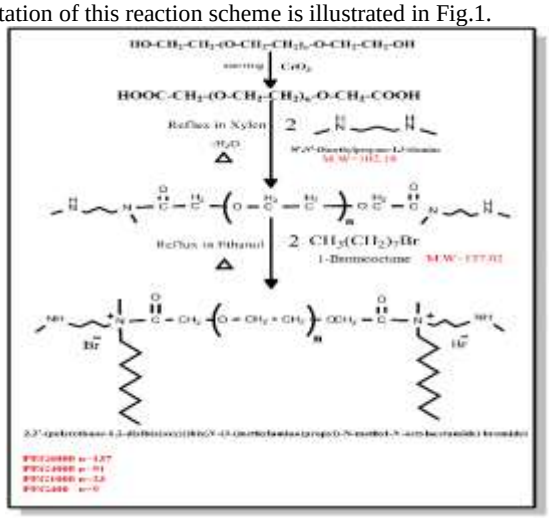

Fig. 1. Preparation mechanism steps for Gemini surfactants PE-Br-400, PE-Br-1000, PE-Br-4000, and PE-Br-6000.

2.2. Tensiometer method.

The Tensiometer method, using the KRÜSS K6 Tensiometer, is an accurate, high-tech way to measure liquid surface tension. This tool is valued in research, quality control, and industry for its precision and adaptability. The KRÜSS K6 Tensiometer works by inserting a platinum ring into the desired liquid. The platinum ring is gently removed, and the force needed for this is measured with high accuracy. The liquid's surface tension is then accurately calculated by examining the force [12]. The synthesized Gemini surfactant compounds' surface tension was measured as a function of surfactant concentration using the platinum ring detachment method (Tensiometer KRÜSS K6). At 25°C, 40°C, and 60°C, the surface tension of the synthesized Gemini surfactants was determined at three different concentrations ($5X10^{-3}$ to $1X10^{-8}$). To get reliable findings, surface tension must be measured at least three concentrations; the mean value is then calculated from these readings until equilibrium values are obtained. Plotting the surface tension against concentration reveals the CMC at a line break (Fig. 2). [13]

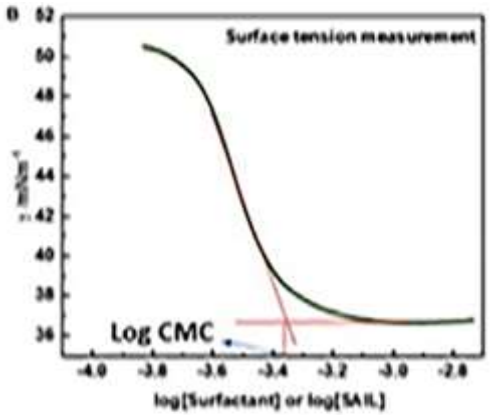

Fig. 2. Surface tension plot

2.3. Mass loss technique by gravimetric

This technique, we can assess the degree of surface coverage (θ) and the efficiency of corrosion inhibition (η_W(%) of synthetic inhibitors on mild carbon steel (MCS) surfaces, which have a form of circular flush disc coupons. The evaluation comprises submerging the coupons for 24 hours at different temperatures (25°C, 50°C, and 70°C) in a corrosive medium containing 1 N HCl solution with various inhibitor concentrations (25, 50, 100, 200, and 400 ppm). Equations (1) and (2) are then applied.

$$\theta = \frac{(W_{Lu} - W_{Li})}{W_{Lu}} \quad \text{..... (1).}$$

$$\eta_W\,(\%) = \theta \text{ X } 100 \quad \text{..... (2).}$$

W_{Lu} and W_{Li} represent the weight loss of flush disk coupons in uncontrolled and inhibited solutions, respectively.

The circular flush disc coupon was sourced from CAPROCO,[14] Its dimensions are Ø 31.8 x 3.2 mm (Ø 1.25 x 1/8") with a surface area of 1.548 mm2 (2.40 in2). Chemical composition analysis was conducted using a mobile optical emission spectrophotometer PMI-MASTER Pro2. The analysis revealed weight percentages of 0.061 C, 0.018 P, 0.054 Mo, 0.18 Mn, 0.017 Al, 0.035 Cr, 0.034 V. The remaining portion of the coupon is composed of Fe.

2.4. Electrochemical techniques

In this electrochemical research, three glass cell electrodes from the Volta Lab PGZ 301 apparatus were utilized [15]. These electrodes comprised a mild steel working electrode (WE), a platinum plate counter electrode (CE) with a surface area of 3 cm², and a saturated calomel reference electrode (SCE) saturated with KCl, maintaining a potential of 0.240 V versus SHE. Data gathering and analysis were facilitated by the Volta Master 4 computer program. The experiments involved subjecting a corrosive electrolyte solution of 1N HCl to various concentrations of manufactured Gemini inhibitors (25, 50, 100, 200, and 400 ppm).

To ensure consistency, three sets of experiments were conducted, and results were obtained using the Nyquist form of Electrochemical Impedance Spectroscopy (EIS) technique, with a frequency range from 1.0 x 10^5 to 1.0 x 10^{-2} Hz and an alternating current voltage of 10 mV. Tafel plot analysis was employed to determine parameters such as corrosion potential (E_{corr}), corrosion current density (i_{corr}), and polarization resistance (Rp) using the potentiodynamic polarization technique. The open-circuit potential (OCP) of the working electrode (WE) was maintained for at least 30 minutes. Electrode potential was scanned from -1000 mV to -200 mV for polarization and impedance curves, with a sweep rate of 2 mV s^{-1}, utilizing the saturated calomel electrode (SCE) [16].

2.5. Theoretical Quantum Chemistry and Simulation of Molecular Dynamics

The structures of the produced Gemini surfactant inhibitors were sketched in Gaussian View 5.0. Theoretical computations in the gas phase were then performed using Gaussian 09W software, which employed Hartree-Fock (HF) theory using Sto-3G base sets. This enabled the geometric structure and single point energy to be computed. The adsorption of these inhibitors on the MCS surface was examined by evaluating several quantum chemical characteristics. These included molecule orbital energies, such as the highest occupied orbit (E_{HOMO}), the lowest unoccupied orbit (E_{LUMO}), and the energy difference between them (ΔE). Chemical descriptors, including chemical hardness (η), absolute electronegativity (χ), dipole moment (μ), global softness (σ), electron affinity (E), ionization potential (I), and electron transfer fraction (ΔN), were studied. These parameters are calculated through the following equations [17].

$$\Delta E = E_{LUMO} - E_{HOMO} \quad (3)$$

$$\eta = \frac{1}{2}(E_{LUMO} - E_{HOMO}) \quad (4)$$

$$X_{inh} = -\frac{1}{2}(E_{LUMO} + E_{HOMO}) \quad (5)$$

$$\mu = -\chi_{inh} \quad (6)$$

$$\sigma = \frac{1}{\eta} \quad (7)$$

$$E = -E_{LUMO} \quad (8)$$

$$I = -E_{HOMO} \quad (9)$$

$$\Delta N = \frac{\phi_{fe} - \chi_{inh}}{2(\eta_{fe} + \eta_{inh})} \quad (10)$$

ϕ denotes the work function of the metal substrate surface. On an iron surface, ϕ_{fe} is 4.81, while mild carbon steel's electronegativity (η_{fe}) is 0 eV.

The computational investigation of the mechanics of Gemini surfactant inhibitors on the Fe (110) surface was conducted using Material Studio 2020 software. Firstly, geometry optimization was carried out employing the forcite tools module with the compass III force field at ultra-fine quality. Subsequently, simulation of the adsorption mechanism was performed via Montecarlo simulation utilizing the adsorption locator tools module with the compass III force field at fine quality. The surface structure of the Fe (110) plane was represented using a three-layer slab model, and the dimensions of the adsorption surface box were consistent across various simulations: (47.0 X 47.0 X 54.1) for PE-Br-400, (148.5 X 148.5 X 104.1) for PE-Br-1000, (347.6 X 347.6 X 324.1) for PE-Br-4000, and (447.6X 447.6 X 454.1) for PE-Br-6000. Additionally, the adsorption process was simulated in the presence of 500 H2O molecules [18].

3. Results and discussion

3.1. characterization of Gemini polyethylene glycol derivative (PEGD) surfactants

The synthetic procedures employed to produce Gemini surfactant inhibitors (PE-Br-400, PE-Br-1000, PE-Br-4000, and PE-Br-6000) are illustrated in Fig.1. The final molecular structures were characterized using FT-IR spectroscopy (Fig.3) and ^{1}H-NMR spectroscopy (Fig.4). In the FT-IR spectra of PE-Br-400, an absorption band at 3446 cm^{-1} corresponding to N-H stretching was observed, along with distinct peaks at 2837 cm^{-1} and 2915 cm^{-1} attributed to symmetric and asymmetric stretching of CH_2 groups. Peaks at 1624 cm^{-1} suggested carbonyl stretching of the amide band, while signals at 1428 cm^{-1} and 1306 cm^{-1} were associated with CH_2 and CH_3 bending, respectively. Additionally, strong peaks at 1076 cm^{-1} and 683 cm^{-1} indicated the presence of ether (C–O–C) and N-H wagging, respectively. Similar spectral features were observed for PE-Br-1000, PE-Br-4000, and PE-Br-6000, with variations in peak positions and intensities [19], [20].

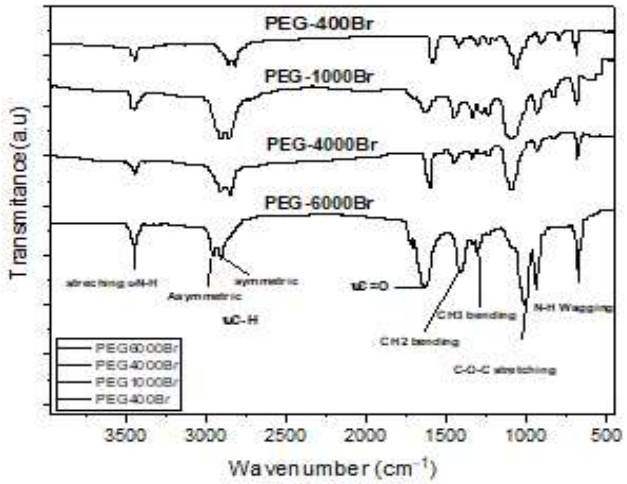

Fig. 3. FTIR of Gemini surfactant inhibitors (PE-Br-400, PE-Br-1000, PE-Br-4000, and PE-Br-6000).

Scheme1 illustrates the molecular structure of the polyethylene glycol derivative (PEGD), and Fig. 4 displays the ^{1}H NMR spectra of PE-Br-400, PE-Br-1000, PE-Br-4000, and PE-Br-6000. The chemical shifts (δ) and corresponding proton multiplicities are provided for each compound in $CDCl_3$.

^{1}H NMR of **PE-Br-400** (Fig. 4i), ($CDCl_3$, δ =7.25): δ 0.63-0.78 (t, 6H, a), 1.03-1.57 (tt, 24H, b), 2.11 (2H, NH,c) 2.71 (quint, 4H, d) , 2.77 (s,6H, e), 2.83 (t,4H, f), 2.77(s,6H,g) 2.95-3.60 (t,36H,h), 3.82-4.08 (t,2H,i). **PE-Br-1000** (Fig. 4ii), ($CDCl_3$, δ =7.25): δ 0.83-0.86 (t, 6H, a), 1.21-1.26 (tt, 24H, b), 2.14 (2H, NH,c) 2.30 (quint, 4H, d) , 2.35 (s,6H, e), 3.08 (t,4H, f), 3.26 (s,6H,g) 3.56-3.73 (t,92H,h), 4.8-5.13 (t,2H,i). **PE-Br-4000** (Fig. 4iii), ($CDCl_3$, δ =7.25): δ 0.82-0.95 (t, 6H, a), 1.16-1.66 (tt, 24H, b), 2.0 (2H, NH, c) 2.13 (quint, 4H, d), 2.31 (s,6H, e), 2.58 (t,4H, f), 2.74(s,6H,g) 3-39-3.74 (t,364H,h), 5.13 (t,2H,i). **PE-Br-6000** (Fig. 4iv), ($CDCl_3$, δ =7.25): δ 0.82-0.85 (t, 6H, a), δ 1.21 (tt, 24H, b), δ 2.13 (2H, NH, c) 2.34 (quint, 4H, d), 2.39 (s,6H, e), 2.59 (t,4H, f), 2.90(s,6H, g) 3-39-3.70 (t, 548H,h), 5.13-5.89 (t,2H,i) [21].

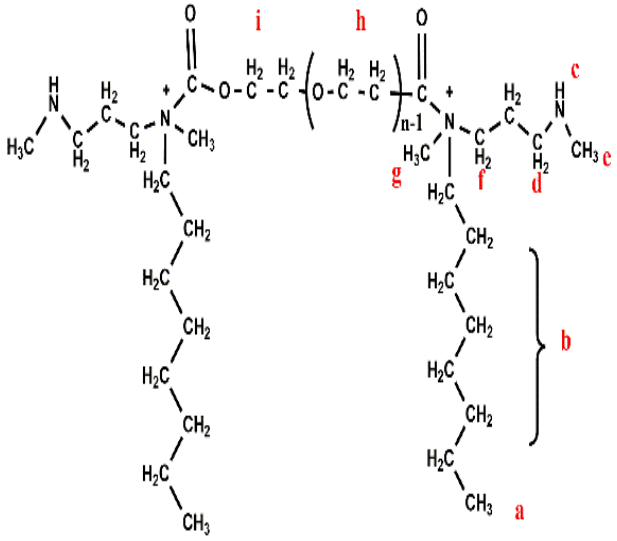

Scheme 1. Molecular structure of polyethylene glycol (PEG) derivative.

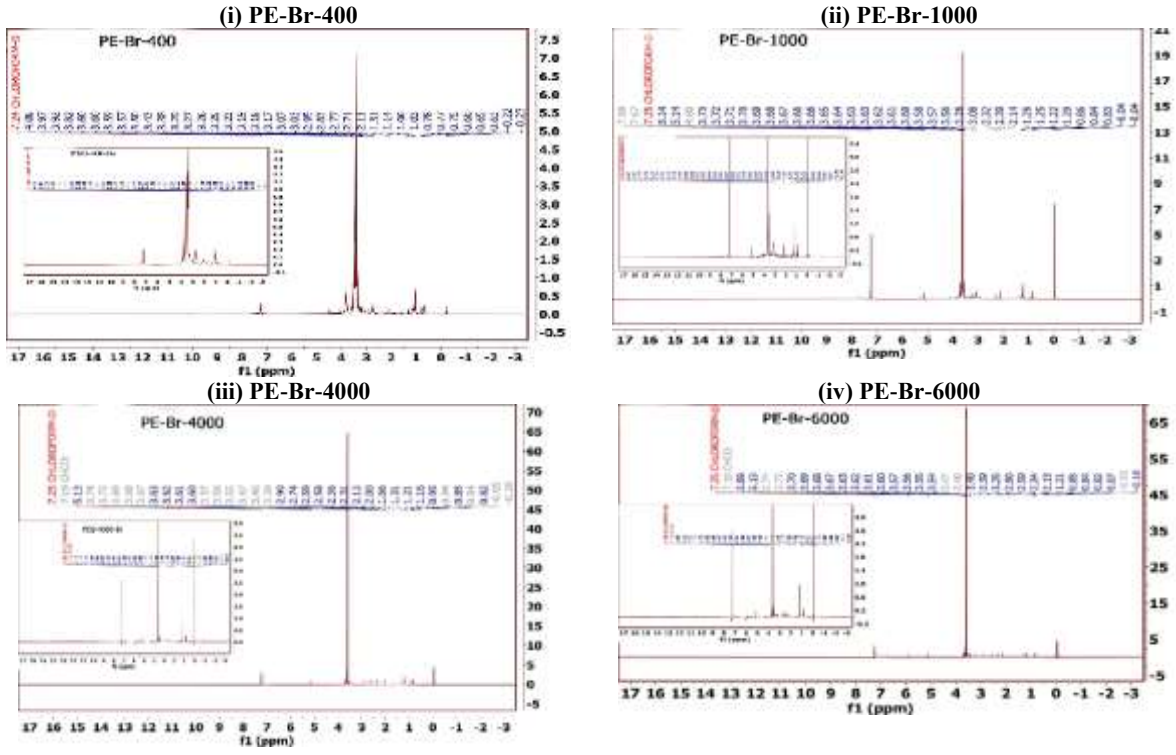

Fig. 4 (i, ii, iii ,iv). 1H-NMR Spectrum of (PE-Br-400, PE-Br-1000, PE-Br-4000, and PE-Br-6000), respectively.

3.2. Determination of Surface-Active Properties.

3.2.1 *surface tension and calculation of critical micelle concentration (CMC).*

Surfactant molecules are characterized by their dual nature: a hydrophobic tail, typically a long carbon chain, and a hydrophilic head. In aqueous solutions, these molecules arrange themselves according to their polarities. The hydrophilic head orients towards the aqueous phase, while the hydrophobic tail aligns at the interface between the gas (air) and liquid phases. This alignment minimizes the repulsive interactions with water molecules, leading to the gradual accumulation of surfactant molecules at the gas-aqueous interface, which results in a decrease in the surface tension of the aqueous phase. This accumulation continues until a specific concentration of surfactant molecules is reached, beyond which excess molecules aggregate to form micelles. This concentration threshold is known as the critical micelle concentration (CMC), marking the onset of micellization. [22]. Figure 5 presents the surface tension profiles of solutions containing synthesized Gemini surfactant compounds (PE-Br-400, PE-Br-1000, PE-Br-4000, and PE-Br-6000) plotted against their concentrations. These profiles exhibit two distinct regions. Initially, there is a consistent decrease in surface tension with increasing surfactant concentration, indicating the adsorption of the synthesized Gemini surfactant compounds at the air-water interface. The slope of this phase reflects the degree of adsorption. In the subsequent region, surface tension values stabilize as concentrations increase, suggesting that no further surfactant molecules are being adsorbed at the air-water interface. The CMC values are identified at the intersection point between these two regions.[23], [24]. Hydrogen bonding is likely to form between water molecules and the head groups of PE-Br-400, PE-Br-1000, PE-Br-4000, and PE-Br-6000 via the oxygen atom of the carbonyl groups. This interaction is expected to enhance hydration at the head group level, thereby reducing repulsive Coulombic forces among charged heads. Additionally, it facilitates connections among the head groups, promoting the formation of surfactant aggregates at lower concentrations.

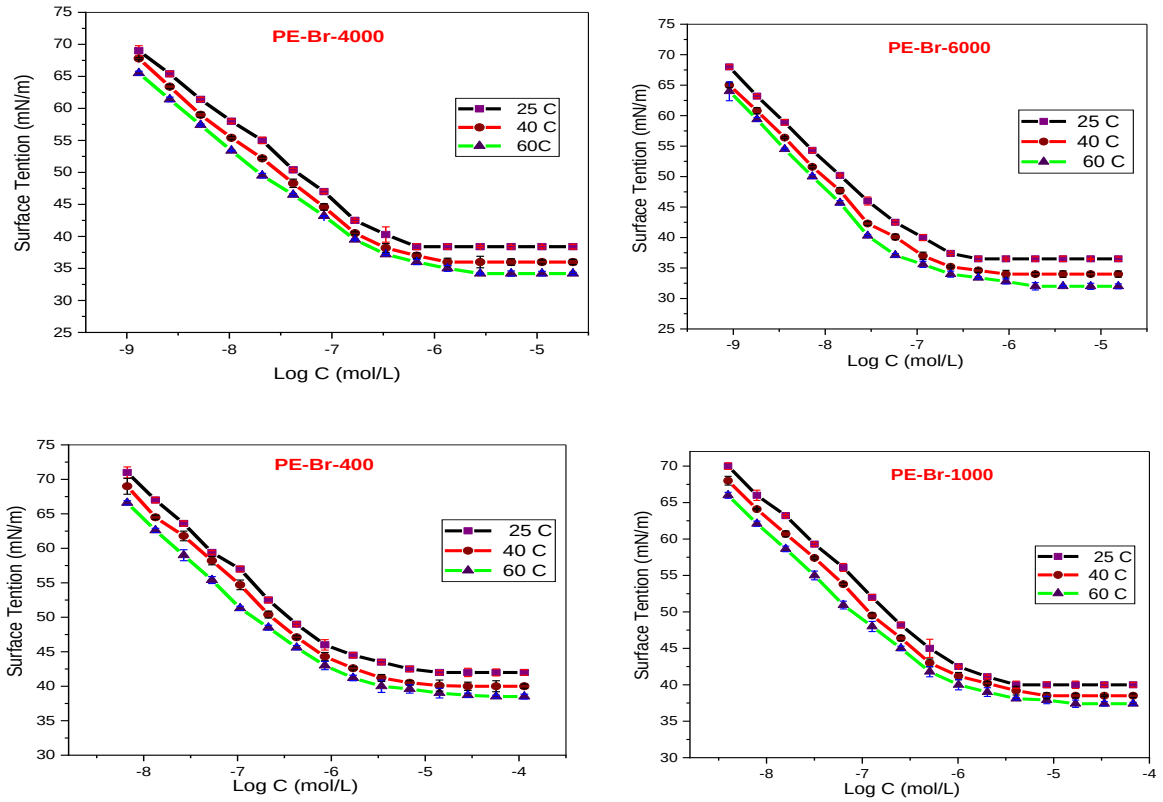

Fig. 5. Surface tension vs. log concentration of the (PE-Br-400, PE-Br-1000, PE-Br-4000, and PE-Br-6000) at different temperature.

The micellization mechanism is influenced by two factors: the repulsion between the hydrophobic tails of surfactant molecules and water molecules, and the repulsion between the charged head groups of the surfactant molecules. Consequently, as the number of repeated ethoxy (O-CH2-CH2-) units increases, the CMC decreases. This is why PE-Br-6000, with the highest number of ethoxy units, shows the lowest CMC value across different temperatures, as illustrated in Table 1.

3.2.1.1 Impact of temperature on CMC

To investigate the thermodynamic properties of micellization, we assessed the critical micelle concentrations (CMCs) of synthetic Gemini polyethylene glycol derivative (PEGD) surfactants at three different temperatures: 25°C, 40°C, and 60°C. The results, presented in Table 1 and Figure 6, indicate that CMC values increase with rising temperature. This temperature dependence of micellization is influenced by two opposing forces. At higher temperatures, micellization is facilitated by a decrease in the hydration level of the head groups, which reduces the repulsive interactions between them. Conversely, at lower temperatures, micellization is inhibited due to the disruption of the structured water surrounding the hydrophobic groups. Within the studied temperature range, the latter effect appears to be more significant, leading to an increase in CMC values as the temperature rises. This trend underscores the complex interplay between hydrophobic and hydrophilic interactions during the micellization process and highlights the importance of temperature in modulating surfactant behavior . [25].

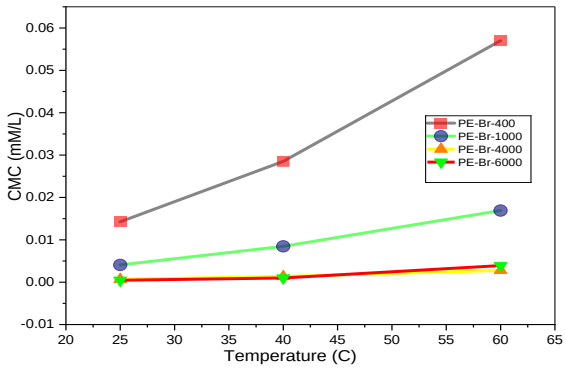

Fig. 6. Temperature (C) vs critical micelle concentration (mM/L) of PE-Br-400, PE-Br-1000, PE-Br-4000, and PE-Br-6000.

3.2.2. Determination of surface-active properties.

The surface properties of synthesized Gemini surfactants, including their efficiency (π_{cmc}), effectiveness (PC_{20}), maximum Surface Excess (Γ_{max}), and minimum surface area per molecule (A_{min}), are pivotal in determining their suitability for applications in the oil and gas field. The maximum surface excess, indicating the quantity of surfactants adsorbed and accumulated at the air/water interface, was determined at various temperatures utilizing the Gibbs equation of the adsorption process). (equation11),

Γ_{max}=1/ -2.303 nRT ($\partial\gamma/\partial$log C)……(11)

This equation involves the number of ionic species "n" accumulating at the air-water interface, where "n" equals 3 for synthesized Gemini surfactants, "R" is the gas constant (8.314 J mol^{-1} k^{-1}), "T" represents the temperature in Kelvin (equal to 273 plus the Celsius temperature), and "γ" denotes the surface tension. The data in Table 1 demonstrates that the order of maximum surface excess (Γ_{max}) values across all temperatures (25°,40°, 60° C) is PE-Br-6000 > PE-Br-4000 > PE-Br-1000 > PE-Br-400. This ordering is attributed to the greater repulsion force between the charged headgroups of the PE-Br-6000 surfactant molecule compared to others, with increasing temperature correlating with decreased maximum surface excess.

The effectiveness (π_{cmc}) of Gemini surfactants can be determined using equation 12.

$\pi_{CMC} = \gamma_o - \gamma_{CMC}$…… (12)

which calculates the difference between the surface tension of distilled water (γ_o) and the Gemini surfactant solution (γ_{CMC}) at its critical micelle concentration. Higher π_{cmc} values indicate greater surface activity and efficiency. According to Table 1, PE-Br-6000 demonstrates the highest efficiency among the synthesized Gemini surfactants. However, with rising temperatures from 25°C to 60°C, the effectiveness values for all four Gemini surfactants (PE-Br-400, PE-Br-1000, PE-Br-4000, and PE-Br-6000) consistently decrease, indicating reduced surface activity at higher temperatures.

$$A_{min} = \frac{10^{16}}{[\Gamma_{max} . N_A]} \ldots\ldots\ldots\ldots\ldots\ldots\ldots\ldots\ldots\ldots\ldots (13).$$

where N_A is Avogadro's number (6.023×10^{23}), is detailed in Table 1. The data analysis shows that the minimum surface area (Amin) per molecule increases with higher measurement temperatures, indicating that the number of molecules at the interface decreases as temperature increases. [26].

3.2.3 Examining the thermodynamic properties of synthesized molecules.

Using Gibbs equations (14, 15), one can determine the standard free energies of the micellization and adsorption processes (ΔG^0_{mic} &ΔG^0_{ads} respectively) for synthesized Gemini surfactants (PE-Br-400, PE-Br-1000, PE-Br-4000, and PE-Br-6000) at different temperatures (25°, 40°, and 60° C).

ΔG^o_{mic} = 2.303RT Ln CMC …….. (14)

$\Delta G^o_{ads} = \Delta G^o_{mic} - (0.6\, \pi_{CMC}\, A_{min})$ …….. (15)

Negative values for both ΔG^o_{mic} and ΔG^o_{ads} in Table 2 indicate spontaneous occurrence of adsorption and micellization processes of the synthesized surfactants. As temperature rises, ΔG^o_{ads} becomes more negative than ΔG^o_{mic}, indicating superior adsorption process at the air/water interface. Consequently, the solution exhibits greater thermodynamic stability Positive values from the difference between micellization and adsorption standard free energy (ΔG^o_{mic} - ΔG^o_{ads}) suggest a higher tendency for synthetic Gemini surfactant molecules to adhere to the air-water interface rather than form micelles. The change in entropy associated with micellization and adsorption can be determined using equations (16) and (17),

$-\Delta S^o_{mic} = \Delta G^o_{mic} / \Delta T$……..... (16)
$-\Delta S^o_{ads} = \Delta G^o_{mic} / \Delta T$……..…. (17)

Where ΔS^o_{mic} & ΔS^o_{ads} are entropy of micellization and adsorption process, respectively.

In all cases, the change in entropy remains consistently positive, indicating that the aggregation of synthesized Gemini surfactant molecules favours increased entropy. However, it is evident from the tabulated data (Table 2) that these values decrease with rising temperature.

Table 1: The critical micelle concentration (CMC), effectiveness (πc_{mc}), efficiency (Pc_{20}), maximum surface excess (Γ_{max}), and minimum surface area (A_{min}) of the (PE-Br-400, PE-Br-1000, PE-Br-4000, and PE-Br-6000) were measured at temperatures of 25^0, 40^0, 60^0 C.

Compounds	T	CMC	π_{cmc}	Pc_{20}	Γ_{max}	A_{min}
	C°	mM/l	$mN.m^{-1}$	M/L $X10^{-7}$	$mol.cm^{-2}$ $X10^{-11}$	nm^2
PE-Br-400	25	1.4E-02	27.0	0.3872	4.14	404.0
	40	2.9E-02	29.0	0.2393	3.91	424.1
	60	5.7E-02	29.3	0.1225	3.48	476.7
PE-Br-1000	25	4.1E-03	29.0	0.2347	4.45	373.3
	40	8.5E-03	30.5	0.1271	4.03	412.1
	60	1.7E-02	30.6	0.0635	3.60	460.7
PE-Br-4000	25	6.7E-04	32.6	0.0419	4.48	370.8
	40	1.3E-03	33.0	0.0330	4.03	385.2
	60	2.8E-03	33.8	0.0117	3.77	417.1
PE-Br-6000	25	4.6E-04	33.5	0.0147	4.53	381.7
	40	9.3E-04	35.0	0.0120	4.08	407.3
	60	1.9E-03	36.0	0.0072	3.82	428.6

This decrease in self-aggregation tendencies can be attributed to increased molecule mobility at higher temperatures, leading to reduced self-aggregation. Positive values of ΔS^o_{mic} can be interpreted by the disintegration of flickering clusters encapsulating surfactant molecules' alkyl chain tails and the resulting increase in unpredictability within the micellar core's alkyl chain tails. Two main factors contribute to the increase in micellization entropy within an aqueous solution. Firstly, the formation of H_2O molecules surrounding surfactant molecules adds to the system's order. Micellization involves the removal of surfactant molecules from the aqueous solution to the micelle, increasing the system's entropy due to the disruption of water molecule assembly. Secondly, Surfactant molecules' hydrophobic chains are more flexible in rotation in the non-polar micelle interior than they are in the watery environment. In essence, as surfactant molecules migrate from the watery environment into the micelle, the configurational entropy of their hydrophobic chains increases.[27], [28].

Table 2: thermodynamic properties of adsorption and micellization process for PE-Br-400, PE-Br-1000, PE-Br-4000, and PE-Br-6000 at 298 K0, 313 K0 and 333 K0 C.

Compounds	T	ΔG^0_{mic}	ΔG^0_{ads}	ΔG^0_{mic}- ΔG^0_{ads}	ΔS_{mic}	ΔS_{ads}	ΔH_{mic}	ΔH_{ads}
	K°	kJ . mol^{-1}	$kJ.mol^{-1}$	$kJ.mol^{-1}$	kJ. $mol^{-1}.K^{-1}$	kJ. $mol^{-1}.K^{-1}$	$Kcal.mol^{-1}$	$Kcal.mol^{-1}$
PE-Br-400	298	-27.55	-34.08	6.52	--	--	--	--
	313	-27.97	-35.38	7.41	0.028	0.09	-19.28	-8.23
	333	-28.16	-36.57	8.41	0.017	0.07	-22.43	-12.86
PE-Br-1000	298	-30.79	-37.31	6.52	--	--	--	--
	313	-31.22	-38.79	7.57	0.029	0.099	-22.20	-7.87
	333	-31.59	-40.08	8.49	0.023	0.079	-24.01	-13.74
PE-Br-4000	298	-35.25	-42.52	7.28	--	--	--	--
	313	-35.81	-44.00	8.18	0.038	0.098	-23.95	-13.27
	333	-36.16	-45.13	8.96	0.026	0.074	-27.42	-20.37
PE-Br-6000	298	-36.33	-43.73	7.40	--	--	--	--
	313	-36.88	-45.46	8.59	0.036	0.116	-25.47	-9.28
	333	-37.09	-46.51	9.42	0.022	0.07933	-29.89	-20.٤8

The enthalpy changes during micellization and adsorption processes are calculated using equations (18) and (19), respectively.

$-\Delta H^o_{mic}=\Delta G^o_{mic}$ +TΔS^o_{mic}……..(18)

$-\Delta H^o_{ads}= \Delta G^o_{ads} + T\Delta S^o_{ads}$……..……. (19)

Where $\boldsymbol{\Delta H^o_{mic}}$& $\boldsymbol{\Delta H^o_{ads}}$ are enthalpy of micellization and adsorption process, respectively.

The negative enthalpy changes indicate exothermic processes, which enhance both micelle formation and stability. A lower negative enthalpy change can reduce the critical micelle concentration (CMC) of surfactants, indicating increased interfacial activity. $\boldsymbol{\Delta H^o_{mic}}$ values decrease with rising temperature, suggesting a preference for adsorption over micellization in the surfactant solution. PE-Br-6000 shows a more negative enthalpy change compared to PE-Br-4000, PE-Br-1000, and PE-Br-400, indicating higher interfacial activity[29], [30].

3.3. Assessments of corrosion inhibition.

The corrosion process denotes the dissolution of metal within a corrosive media, subject to monitoring through various methodologies including gravimetric and electrochemical assessments.

3.3.1 Determining corrosion inhibition through Gravimetric Measurements.

This approach is a commonly employed and cost-effective methodology since measures the changes in the weight of mild carbon steel (MCS) specimens at different time intervals. While accurately measuring initial and final metal weights is important, relying solely on weight loss data has limitations in monitoring corrosion. The mass loss can be evaluated using equation (20).

$W_L = \frac{\Delta W}{A}$..... (20)

where W_L is the mass loss per unit area, A is the metal sample's surface area.

Weight loss measurements indicate the overall decrease in sample weight without considering differences in metal surface area during corrosion, which cause bigger surfaces to lose more weight than smaller ones. To provide a full assessment of corrosion extent, the corrosion rate (CR) is an important quantity. Equation (21) can be used to determine CR, which is an estimate of the quantity of metal dissolved per unit area of metal surface over a specified time.

CR=$\frac{W_L}{t}$……..…….... (21)

Where t is exposure time. Corrosion rate determination provides it easier to evaluate the inhibition efficiency of synthesized

Gemini surfactant inhibitors, which reflects their effectiveness in inhibiting corrosion and protecting the metal surface in corrosive situations like 1 N HCl solution. Table 3 details the impact of multiple factors, such as inhibitor concentration and polyethylene glycol chain length, on the evaluated inhibitors' corrosion rate and inhibition effectiveness at varying temperatures (25°, 55°, and 70°C).

3.3.1.1 Impact of inhibitor concentration on mild carbon steel corrosion.

It is evident that when the inhibitor concentration rises, the corrosion rate (CR) decreases, and inhibition efficiency rises in tandem. The adsorption of inhibitors at the interface between mild carbon steel (MCS) and 1N HCl solution is responsible for reducing the corrosion process on MCS. The contact between the metal surface and corrosive ions is reduced when inhibitor molecules are adsorbed onto the surface of Table 3 shows that the PE-Br-6000 inhibitor has the highest inhibition efficiency at 25 ppm, with an impressive 86.4%, when comparing the results of inhibition efficiency at 25 ppm by weight after 24 hours. On the other hand, the inhibition efficacy rises to 98.3% at 25°C when the PE-Br-6000 inhibitor concentration is increased to 400 ppm [31].

3.3.1.2 Influence of polyethylene glycol chain length on the corrosion of mild carbon steel.

Corrosion inhibition is the process of absorbing inhibitors onto the metal surface, which is promoted by the interaction of oxygen atoms' lone electron pairs with positively charged centers on the substrate. The adsorbed oxygen atoms are most likely aligned with the surface of mild carbon steel, creating a coating that decreases the metal's reactivity during electrochemical corrosion reactions. The Gemini surfactant inhibitors PE-Br-400, PE-Br-1000, PE-Br-4000, and PE-Br-6000 adsorb at the interface of mild carbon steel and HCl solution, inhibiting acid dissolution.

Table 3: Gravimetric parameters for PE-Br-400, PE-Br-1000, PE-Br-4000, and PE-Br-6000 at 25°, 55°, and 70°C after 24 hours.

Inhibitor	Conc. inhibitor (ppm) in 1N HCl	Corrosion rate k (mg $cm^{-2}h^{-1}$)			θ			η_w (%)					
		25^0 C	55^0 C	70^0C	25^0 C	55^0 C	70^0 C	25^0 C		55^0 C		70^0C	
PE-Br-400	**blank**	**0.94± 0.06**	**2.21± 0.11**	**4.37± 0.4**	**…..**	**…...**	**…..**	**…..**	**…..**	**…..**	**…..**	**…..**	**…..**
	25	**0.31± 0.02**	**0.57± 0.13**	**1.11± 0.23**	**0.68**	**0.74**	**0.74**	**67.6%**	**2.80%**	**74.0%**	**8.10%**	**74.5%**	**7.50%**
	50	**0.29± 0.02**	**0.54± 0.07**	**1.03± 0.17**	**0.69**	**0.76**	**0.76**	**69.1%**	**2.30%**	**75.8%**	**4.40%**	**76.3%**	**2.10%**
	100	**0.26± 0.01**	**0.49± 0.07**	**0.95± 0.11**	**0.73**	**0.78**	**0.78**	**72.9%**	**1.90%**	**77.7%**	**4.90%**	**78.3%**	**0.80%**
	200	**0.21± 0.02**	**0.41± 0.1**	**0.75± 0.23**	**0.78**	**0.81**	**0.83**	**78.2%**	**2.50%**	**81.4%**	**3.00%**	**82.8%**	**3.90%**
	400	**0.12± 0.02**	**0.29± 0.06**	**0.4± 0.15**	**0.87**	**0.88**	**0.91**	**87.4%**	**2.60%**	**87.6%**	**2.70%**	**90.8%**	**4.60%**
PE-Br-1000	**25**	**0.25 ± 0.04**	**0.44± 0.05**	**0.9± 0.2**	**0.74**	**0.8**	**0.79**	**73.9%**	**4.00%**	**80.2%**	**2.70%**	**79.4%**	**6.70%**
	50	**0.24± 0.02**	**0.42± 0.07**	**0.85± 0.18**	**0.75**	**0.81**	**0.81**	**75.0%**	**2.40%**	**80.9%**	**2.60%**	**80.5%**	**5.80%**
	100	**0.21+ 0.02**	**0.375± 0.03**	**0.76± 0.09**	**0.78**	**0.83**	**0.83**	**77.9%**	**1.40%**	**82.9%**	**1.30%**	**82.7%**	**1.80%**
	200	**0.17+ 0.02**	**0.299± 0.04**	**0.6± 0.29**	**0.82**	**0.87**	**0.86**	**82.4%**	**1.90%**	**86.6%**	**1.50%**	**86.1%**	**7.20%**
	400	**0.09± 0.02**	**0.18± 0.03**	**0.3± 0.05**	**0.9**	**0.92**	**0.93**	**90.0%**	**1.60%**	**92.0%**	**1.00%**	**93.2%**	**0.60%**
PE-Br-4000	**25**	**0.21+ 0.04**	**0.35± 0.04**	**0.74± 0.2**	**0.78**	**0.84**	**0.83**	**77.5%**	**4.40%**	**84.1%**	**1.90%**	**83.1%**	**2.70%**
	50	**0.195+ 0.02**	**0.33± 0.04**	**0.7± 0.15**	**0.79**	**0.85**	**0.84**	**79.3%**	**2.40%**	**85.0%**	**2.40%**	**84.0%**	**1.90%**
	100	**0.175± 0.02**	**0.28± 0.04**	**0.61± 0.31**	**0.81**	**0.87**	**0.86**	**81.4%**	**2.30%**	**87.2%**	**1.40%**	**86.1%**	**5.90%**
	200	**0.14± 0.02**	**0.22± 0.02**	**0.47± 0.11**	**0.85**	**0.9**	**0.89**	**85.4%**	**2.40%**	**90.1%**	**0.70%**	**89.2%**	**2.90%**
	400	**0.07± 0.07**	**0.11± 0.02**	**0.21± 0.11**	**0.93**	**0.95**	**0.95**	**92.6%**	**0.20%**	**94.9%**	**0.80%**	**95.1%**	**3.00%**
PE-Br-6000	**25**	**0.16± 0.05**	**0.28± 0.06**	**0.61± 0.26**	**0.83**	**0.87**	**0.86**	**83.0%**	**4.30%**	**87.2%**	**3.30%**	**86.1%**	**5.70%**
	50	**0.145± 0.05**	**0.26± 0.1**	**0.57± 0.14**	**0.84**	**0.88**	**0.87**	**84.2%**	**4.80%**	**88.1%**	**5.30%**	**87.1%**	**4.20%**
	100	**0.115± 0.05**	**0.225± 0.01**	**0.48± 0.31**	**0.87**	**0.89**	**0.89**	**87.0%**	**5.80%**	**89.4%**	**0.60%**	**89.1%**	**8.20%**
	200	**0.09± 0.04**	**0.16± 0.06**	**0.32± 0.2**	**0.91**	**0.93**	**0.93**	**90.7%**	**3.60%**	**92.8%**	**2.80%**	**92.6%**	**5.40%**
	400	**0.04± 0.02**	**0.06± 0.04**	**0.09± 0.01**	**0.96**	**0.98**	**0.98**	**95.5%**	**1.50%**	**97.5%**	**2.10%**	**98.0%**	**0.40%**

The corrosion inhibition efficiency of the surfactants follows this order: PE-Br-6000 > PE-Br-4000 > PE-Br-1000 > PE-Br-400. This is attributed to the different lengths of the polyethylene glycol chains. The ethylene glycol units enhance lone pair and ion exchange interactions, facilitating adsorption. The hydrophobic carbon chains of the surfactant molecules face the aqueous medium. [24], [31].

3.3.2 Determining corrosion inhibition through electrochemical measurements.

In comparison to the gravimetric methodology, this approach to calculating the corrosion rate of the MCS surface is thought to offer a significant advantage in terms of speed of measurement. Typical polarization curves that show how carbon steel behaves in a 1 N HCl solution both with and without different amounts of the artificially produced Gemini surfactant inhibitors are shown in Fig. 7. Increased inhibitor concentrations corresponded to higher levels of inhibition efficiency, indicating a deceleration in the reduction of hydrogen ions, notably during the hydrogen evolution process, alongside a reduction in anodic dissolution. PE-Br-6000 exhibited remarkable inhibition efficiency at 89.3%, surpassing other inhibitors, possibly due to its longer chain of ethylene units.

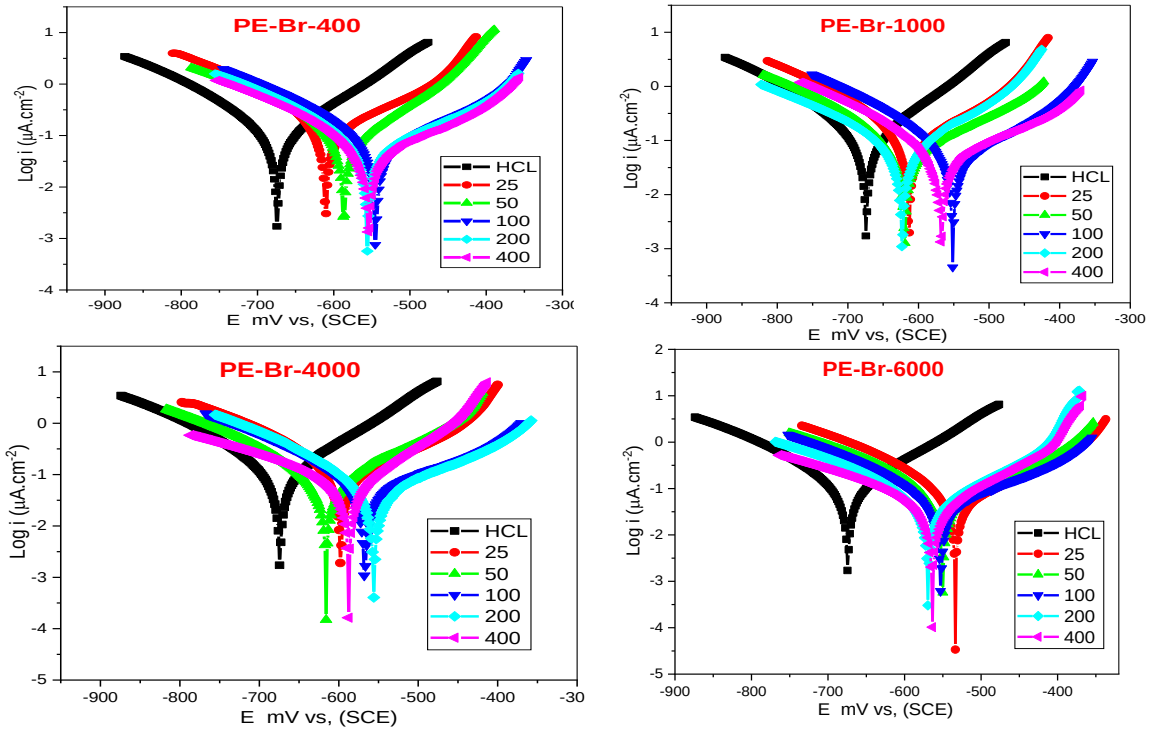

Fig. 7 Polarization curves for PE-Br-400, PE-Br-1000, PE-Br-4000, and PE-Br-6000 in 1 N HCl electrolyte, without and with various concentrations.

This enhanced efficacy was especially prominent at inhibitor concentrations of 400 ppm [32].Another technique used to investigate the corrosion inhibition of inhibitors is electrochemical impedance spectroscopy (EIS). This method utilizes electrical circuits to analyze current responses in redox reactions and fits them to simulation data employed in the study of inhibitor inhibition. The electrical circuit model utilized in this investigation is depicted in Fig. 8.

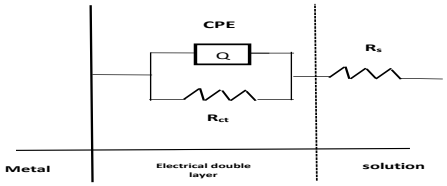

Fig. 8. electrical circuit model for PE-Br-400, PE-Br-1000, PE-Br-4000, and PE-Br-6000

Periodic current and potential signals, with a phase-angle shift (ϕ) spanning from 0 to 90 degrees, oscillate synchronously in an EIS. Equations 24 and 25 state that the application of a sinusoidal potential signal (E) causes a commensurate current response (I) within a particular frequency range.

$$E_t = E_0 \sin(\omega t) \quad \text{(24)}$$

$$I_t = I_0 \sin(\omega t + \phi) \quad \text{(25)}$$

Impedance Z is derived from Ohm's equation derivative (Equation 26,27).

$$Z = \frac{E_t}{I_t} = \frac{E_0 \sin(\omega t)}{I_0 \sin(\omega t + \phi)} \quad \text{(26)}$$

$$Z = Z_0 \frac{\sin(\omega t)}{\sin(\omega t + \phi)} = Z_{re}(\omega) + jZ_{imaginary}(\omega) \quad \text{(27)}$$

The electrochemical impedance spectroscopy (EIS) technique can be represented graphically in two ways. For example, the Nyquist plot (Fig. 9) displays the imaginary impedance ($Z_{imaginary}$) on the y-axis and the real impedance (Z_{real}) on the x-axis. The Bode figure (Fig. 10) depicts the frequency of the applied potential on the x-axis, and the magnitude |Z| and phase shift angle (ϕ) on the y-axis. EIS is commonly used to evaluate the corrosion of a metallic working electrode (WE) in aqueous solutions, usually with a reference electrode (RE) and a polarizable counter electrode (CE). In electrochemical impedance spectroscopy (EIS) experiments, the behavior of the double layer may deviate from ideal capacitor behavior. Therefore, the

Constant Phase Element (CPE) is used to replace the double layer capacitor (Cdl) in the equivalent circuit model. This allows us to calculate the CPE impedance (ZCPE) using the following formula.

$$Z_{CPE} = \frac{1}{Y_0 (j\omega)^n} \text{..... (28).}$$

where Y_0 represents the magnitude of the CPE, j is the imaginary number ($j^2 = -1$), and n denotes the phase shift caused by the inhomogeneities of the electrical double layer. A value of n=0 indicates pure resistance, while n=1 signifies behavior akin to that of an ideal capacitor.

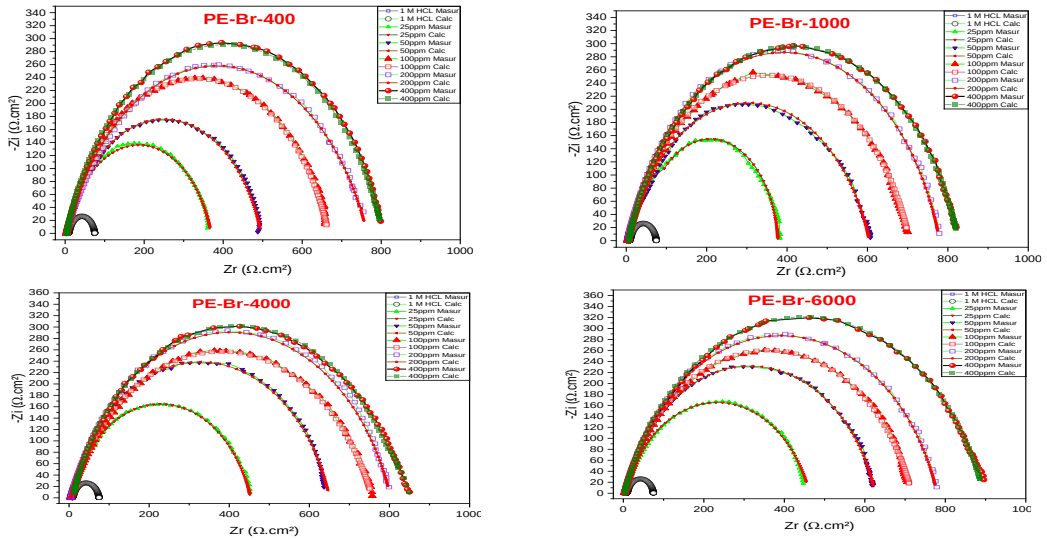

Fig.9. Nyquist diagram for PE-Br-400, PE-Br-1000, PE-Br-4000, and PE-Br-6000.

Table 4: Linear polarization results PE-Br-400, PE-Br-1000, PE-Br-4000, and PE-Br-6000 inhibitors in 1N HCl.

Inhibitors	Concentration PPM	R_p Ω·cm²	$-E_{corr}$ (mV)	i_{corr} (μA.cm⁻²)	βa (mV dec⁻¹)	-βc (mV dec⁻¹)	η_p (%)
PE-Br-400	Blank	62.5	666.9	569.1± 6.2	107.1	159.8	
	25	217.7	554.0	264.9± 2.8	233.3	161.4	53.5%± 0.62%
	50	204.5	555.4	173.2± 6.3	109.5	183.6	69.6%± 1.31%
	100	306.3	544.8	133.2± 8.8	226.2	170.5	76.6%± 1.79%
	200	300.5	586.6	98.3± 3.7	236.3	160.8	82.7%± 0.84%
	400	318.3	610.4	86.3± 5.5	234.8	174.4	84.8%± 1.12%
PE-Br-1000	25	396.9	613.5	231.8± 8.5	129.4	180.4	59.3%± 1.39%
	50	319.5	623.0	145.4± 3.9	270.2	190.7	74.4%± 0.94%
	100	313	551.1	117± 7.8	197.4	172	79.4%± 1.47%
	200	452.3	619.6	97.5± 6.1	203.3	191.1	82.9%± 1.21%
	400	585.7	-610.4	84± 4.4	285.7	173	85.2%± 0.92%
PE-Br-4000	25	189.5	587.4	208.3± 7.8	239.9	171.6	63.4%± 1.73%
	50	268.7	555.8	140.3± 9.3	193.3	178.9	75.3%± 1.58%
	100	379.8	567.2	114.9± 7.6	230.4	177.1	79.8%± 1.50%
	200	358.1	616.0	96.1± 6.2	245.2	167.5	83.1%± 1.26%
	400	791.8	597.6	80.4± 5.3	126.9	229.8	85.9%± 0.96%
PE-Br-6000	25	189.5	563.6	161.5± 7.7	197.1	173.8	71.6%± 1.63%
	50	268.7	569.3	138.6± 7.0	206.9	190	75.6%± 1.44%
	100	379.8	552.8	107.5± 6.5	250.5	176.8	81.1%± 1.34%
	200	358.1	549.7	95.2± 4.7	190.9	193.2	83.3%± 0.99%
	400	791.8	533.5	60.8± 5.4	145.9	213.9	89.3%± 1.02%

The impedance of the equivalent circuit (Z) can be determined using the equation (29).

$$Z = Rs+\frac{1}{Y_0 (j\omega)^n+\frac{1}{R_{ct}}} \text{ ……..(29)}$$

which can be further simplified to:

$$[Zre -(Rs+\frac{R_{ct}}{2})]^2+Z_{img}^2=(\frac{R_{ct}}{2})^2 \text{ ……..(30).}$$

The presence of capacitive loops within all semicircles at higher frequencies in the Nyquist plot (Fig. 9) suggests the existence of a capacitive layer on the working electrode (WE) surface. This indicates that charge transfer resistance (R_{ct}) predominantly regulates reactions occurring at the working electrode surface interface under acidic corrosive conditions. With increasing concentrations of synthetic Gemini surfactant inhibitors (PE-Br-400, PE-Br-1000, PE-Br-4000, and PE-Br-6000), the diameter of the semicircles is increase. The inhibition efficiency (η_E) calculated using the equation (31).

$$\eta_E= \frac{R_{ct(blank)} -R_{ct(inhibitor)}}{R_{ct(blank)}} X\ 100 \text{……. (31)}$$

where $R_{ct(blank)}$ *is charge transfer resistances of acidic solution and* $R_{ct(inhibitor)}$ is charge transfer resistances of inhibited solutions.

According to Figure 9 and Table 5, PE-Br-6000 demonstrates superior efficiency compared to other inhibitors (η_E = 95.6%) at a concentration of 400 ppm [33]. The Bode diagrams illustrate the phase angles of PE-Br-400, PE-Br-1000, PE-Br-4000, and PE-Br-6000 at a concentration of 400 ppm as 65.5°, 67°, 68°, and 70.2°, respectively. This indicates that PE-Br-6000 exhibits the most active inhibition, followed by PE-Br-4000, PE-Br-1000, and PE-Br-400. In Table 5, the lower values of n for inhibited solutions compared to non-inhibited solutions suggest that the Constant Phase Element (CPE) behaves more like a resistance than a non-ideal capacitor in the circuit.

Table 5: EIS results PE-Br-400, PE-Br-1000, PE-Br-4000, and PE-Br-6000 inhibitors in 1N HCl.

Inhibitors	Conc	Rs	Rct	CPE parameters		C_{dl}	η_E
				n	Y_0		
	(PPM)	(Ω cm^2)	(Ω cm^2)		Y0 X10^{-6} (Mho cm^{-2})	μF cm^{-1}	(%)
HCL 1N		5.18	66.67±3.9	0.8906	629.7	426.6	-
PE-Br-400	25	2.44	358.65±7.94	0.8468	574.2	431.4	89.0%±0.14%
	50	1.70	485.71±11.43	0.8143	167.5	94.5	91.9%±.03%
	100	2.70	654.32±12.06	0.8089	90.3	46.3	94%±.06%
	200	2.92	752.29±11.39	0.8006	82.2	41.1	94.8%±0.14%
	400	3.01	795.72±9.37	0.7955	72.1	34.6	95.0%±0.17%
PE-Br-1000	25	2.60	379.33±11.98	0.814	103.9	49.6	89.6%±0.55%
	50	1.97	605.3±9.01	0.8101	92.3	47.0	93.5%±0.12%
	100	2.61	698.0±7.37	0.7953	89.2	43.6	94.3%±0.15%
	200	3.64	775.13±7.23	0.7933	78.1	37.6	94.9%±0.1%
	400	5.23	815.5±10.78	0.791	67.4	31.3	95.2%±0.06%
PE-Br-4000	25	2.72	448.67±6.66	0.8049	97.6	45.7	91.2%±0.11%
	50	2.77	633.6±8.51	0.7617	80.4	31.7	93.8%±0.14%
	100	2.92	753.3±10.5	0.7935	75.3	35.7	94.8%±0.06%
	200	3.01	795.67±4.92	0.7888	71.4	33.1	95.0%±0.09%
	400	11.54	838.5±10.33	0.7749	64.9	27.9	95.3%±0.08%
PE-Br-6000	25	4.24	443.17±6.71	0.8031	94.1	43.2	91.1%±0.09%
	50	2.45	618.67±10.97	0.7952	75.3	34.2	93.6%±0.15%
	100	2.53	702.33±9.45	0.7588	73.3	28.5	94.4%±0.21%
	200	3.64	775.10±14.97	0.7292	68.3	22.9	94.9%±0.22%
	400	2.65	895.6±10.17	0.6948	37.5	8.4	95.6%±0.07%

Moreover, the Y_0 values and double layer capacitance (C_{dl}) values decrease in inhibited solutions compared to uninhibited solutions, with a further decrease observed at higher concentrations of synthesized Gemini surfactant inhibitors, with PE-Br-6000 showing the highest decrease followed by PE-Br-4000, PE-Br-1000, and PE-Br-400.

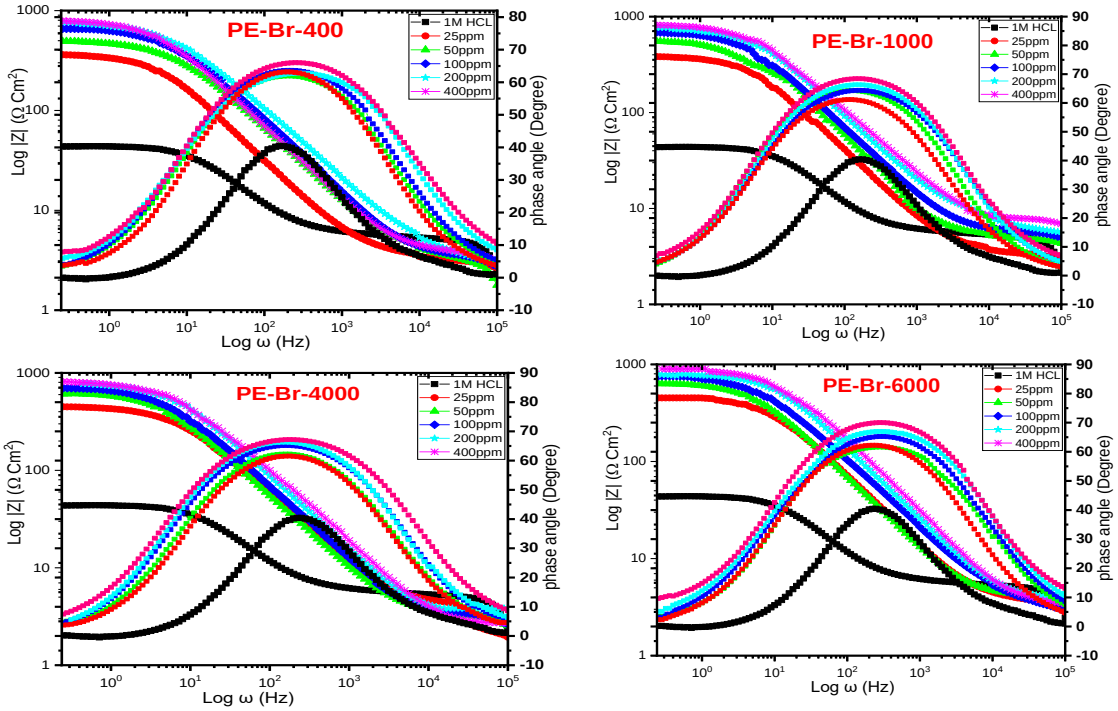

Fig.10. Bode plots for PE-Br-400, PE-Br-1000, PE-Br-4000, and PE-Br-6000.

3.3.3 Understanding adsorption mechanisms on metal surface.

In water-based environments, corrosion inhibitors can adsorb on metallic surfaces via physical (physisorption), chemical (chemisorption), or a mixture of the two (physiochemical adsorption) methods. In this study, chemisorption is identified as the predominant process, characterized by electron transfer between metal and inhibitor particles. Donation refers to the transfer of electrons from the occupied d-orbital of the metal to the cationic nitrogen in the inhibitor, while retro-donation involves the exchange of electrons from the lone pair of oxygen atoms in the inhibitor's ethylene glycol units to the vacant d-orbital of the metal. These interactions, encompassing both donations and retro-donations, often synergize, indicating a mutually beneficial relationship. These terms elucidate the electron exchange between metal and inhibitor substances. The presence of steric hindrance at the terminals of the inhibitors weakens the donation process. Furthermore, these molecules exert electrostatic forces on metallic surfaces, leading to the physiochemical adsorption of the synthesized inhibitors. Consequently, PE-Br-6000, with its long chain of ethylene oxide, demonstrates stronger adsorption on metal compared to other synthesized inhibitors. Furthermore, Cl^- ions have a key role in the adsorption of organic cations in HCl solution by generating intermediate bridges between the surface and the positive ends of PE-BR-400, PE-BR-1000, PE-BR-4000, and PE-BR-6000 molecules (scheme.2).

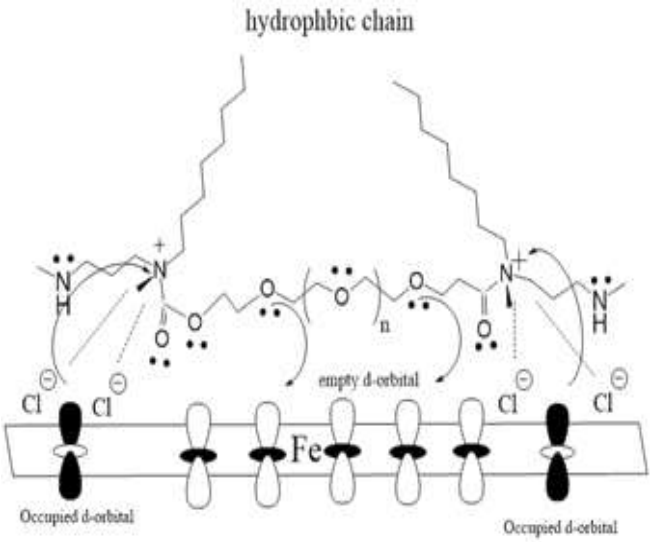

Scheme 2. adsorption process on metallic surface

3.4. Theoretical Quantum Chemistry and Simulation of Molecular Dynamics.

3.4.1 molecular orbitals computation.

Quantum chemical simulations are an efficient method for determining the link between the molecular configurations of produced Gemini surfactant inhibitors and their performance in corrosion inhibition [34]. Through these simulations, valuable insights into the underlying mechanisms of the inhibition process are gained. By utilizing quantum chemical parameters such as energy gap ($\Delta E_{LUMO-HOMO}$), dipole moment (μ), electronegativity (χ), ionization potential (I), electron affinity (A), global hardness (η), softness (σ), and the number of electrons transferred from inhibitor molecules to carbon steel (ΔN), the inhibitory properties of the inhibitors are comprehensively investigated. The E_{HOMO} values serve as indicators of the inhibitor molecules' capability to donate electrons to the metal surface, with higher E_{HOMO} values facilitating easier electron donation from the inhibitor to vacant metal d-orbitals. Conversely, the E_{LUMO} levels are correlated with the inhibitor molecules' capacity to accept electrons, with lower values facilitating the accommodation of additional negative charge by filled metal d-orbitals. According to frontier orbital theory, reactions predominantly occur on the HOMO and LUMO location. Furthermore, the E_{HOMO} and E_{LUMO} values exhibit direct correlations with the ionization potential and electron affinity of organic surfactant molecules. The energy gap ($\Delta E_{LUMO-HOMO}$) serves as an indicator of stability for inhibitors, with smaller values indicating greater stability in inhibitor-metal surface interactions [35]. Fig. 11 illustrates that the electron density distribution of synthetic surfactants predominantly concentrates on specific structural segments, possibly due to the presence of a symmetry plane within their molecular structure.

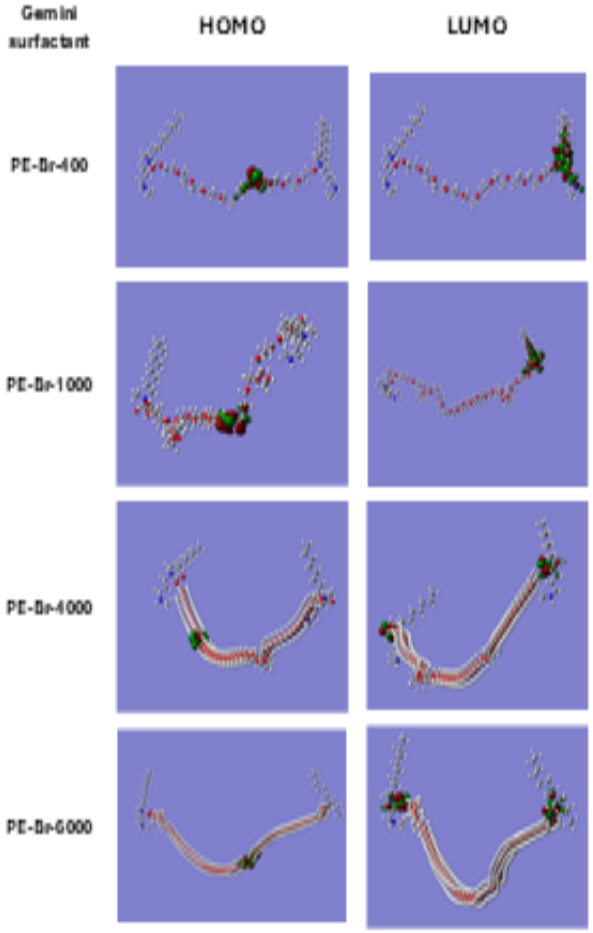

Fig. 11 HOMO and LUMO of PE-Br-400, PE-Br-1000, PE-Br-4000, and PE-Br-6000.

Furthermore, low absolute values of the energy band gap indicate strong inhibitory efficiency since they correspond to lower ionization potentials, which aid in electron removal from outer occupied orbitals. The dipole moment (μ) represents the electronic distribution and polarity of molecules. Elevated dipole moment values contribute to enhanced corrosion inhibition effectiveness. These findings underscore the significance of quantum chemical simulations in advancing our understanding of the molecular mechanisms governing corrosion inhibition processes [36]. This research reported in Table 6 shows that E_{HOMO} values follow the order: PE-Br-6000 > PE-Br-4000 > PE-Br-1000 > PE-Br-400, showing that PE-Br-6000 has the largest electron donation ability due to its longer ethylene glycol chain. This leads to increased adsorption over the mild carbon steel surface, resulting in the maximum inhibitory efficiency. Similarly, E_{LUMO} values follow the order: PE-Br-6000 < PE-Br-4000 < PE-Br-1000 < PE-Br-400, with the lower value of PE-Br-6000 suggesting higher electron receiving ability and concomitant reduction in corrosion of carbon steel.

Table 6: EIS results PE-Br-400, PE-Br-1000, PE-Br-4000, and PE-Br-6000 inhibitors in 1N HCl.

Inhibitors	E_{HOMO}	E_{LUMO}	ΔE_{gab}	I	A	X	η	S (σ)	μ	ΔN
	eV	eV	eV	eV	eV	eV	eV	eV^{-1}	(D)	eV
PE-Br-400	0.3708	0.5277	0.157	-0.371	-0.528	-0.409	0.078	12.75	0.409	1.2
PE-Br-1000	0.3711	0.502	0.131	-0.371	-0.502	-0.415	0.065	15.29	0.415	1.4
PE-Br-4000	0.3842	0.4458	0.062	-0.384	-0.446	-0.437	0.031	32.47	0.437	2.2
PE-Br-6000	0.3918	0.4267	0.035	-0.392	-0.427	-0.449	0.017	57.39	0.449	2.7

Furthermore, the results in Table 6. shows that μ values, determined by equation 6, are in the following order: PE-Br-6000 > PE-Br-4000 > PE-Br-1000 > PE-Br-400. The greater value of PE-Br-6000 indicates enhanced corrosion inhibition and reduced corrosion of the mild carbon steel. PE-Br-6000 has the lowest $\Delta E_{LUMO-HOMO}$ (equation 3), indicating higher adsorptive activity compared to other synthetic Gemini surfactant inhibitors. Lastly, the number of transferred electrons from the inhibitor to the carbon steel surface, indicated by ΔN, correlates with inhibition efficiency. Higher values of ΔN, such as those exhibited by PE-Br-6000, signify greater inhibition efficiencies.

3.4.2 inhibition simulation by molecular dynamics simulation approach.

To assure stability in both total energy and temperature, the study used molecular dynamics simulation (MDS) to reach equilibrium in the simulated system. Figure 12 illustrates the proper adsorption arrangement of synthetic Gemini surfactant inhibitors (PE-Br-400, PE-Br-1000, PE-Br-4000, and PE-Br-6000) on the Fe (110) surface, observed from both top and side views. Visual inspection of the image reveals horizontal adsorption of the inhibitors' head functional groups (- N+-, C=O, -NH) and alkyl chains (C_8H_{17}-) on the Fe (110) surface. Through a physio-chemisorption mechanism, these inhibitors adhere to the metallic surface. The active head functional groups acquire electrons from the occupied orbitals of iron atoms through unoccupied orbitals, while the alkyl chains interact through hydrogen bonding. The adsorption energies (Eads) of the produced Gemini surfactant inhibitors on Fe (110) are determined using equation (32).

$$E_{ads} = -E_{bin} = E_{system} - (E_{Fe} + E_{inh}) \quad \ldots\ldots\ldots\ldots (32)$$

where, E_{Fe} and E_{inh} represent the optimized energies of the Fe (110) surface and the inhibitors, respectively, while E_{bin} indicates the binding energy of the surfactants. E_{system} denotes the total energy of the investigated system.

These simulations are conducted using Monte Carlo computations in fluids containing 500 H2O molecules [37]. The negative E_{ads} values for PE-Br-400, PE-Br-1000, PE-Br-4000, and PE-Br-6000 (-282.3, -453.18, -662.1, and -843.2.49K. Cal/mol, respectively) indicate the spontaneous adsorption of their cationic forms on iron surfaces. Additionally, the low energy values signify a robust interfacial interaction between the inhibitor and Fe (110), leading to stronger inhibition by PE-Br-6000 compared to PE-Br-400, PE-Br-1000, and PE-Br-4000. These modeling outcomes agree with experimental observations, suggesting that our compound exhibits superior inhibitory activity for mild carbon steel [38].

inhibitors	Vacuum phase		Aquatic phase	
	Side view	Top view	Side view	Top view
PE-Br-400	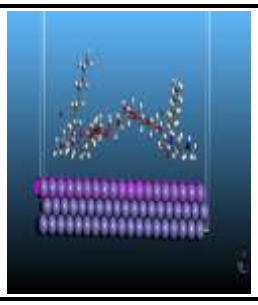	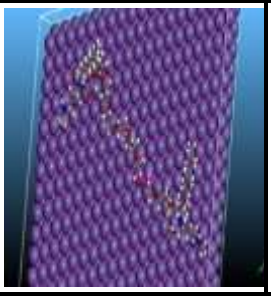	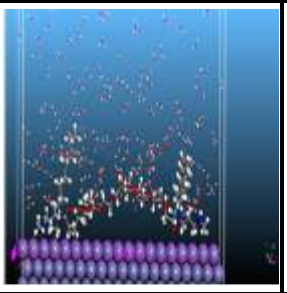	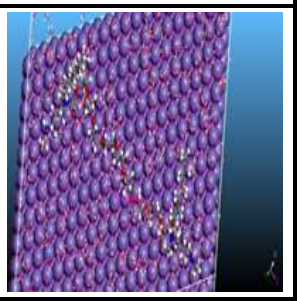
PE-Br-1000				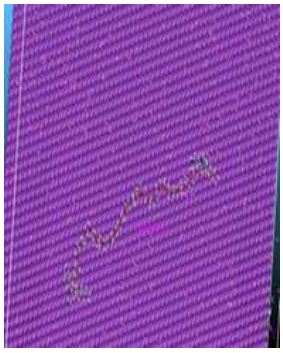
PE-Br-4000	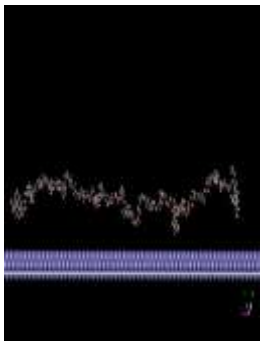	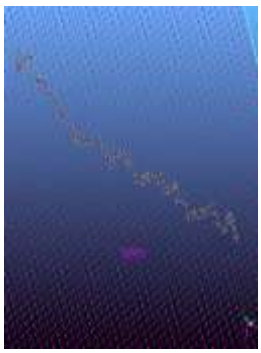	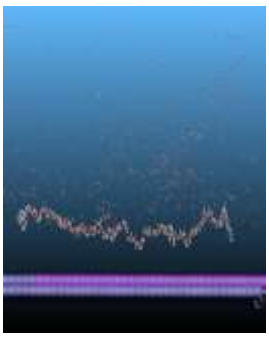	
PE-Br-6000	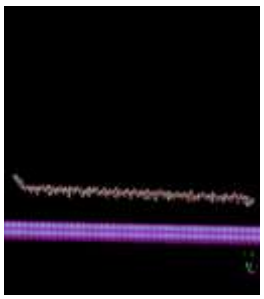		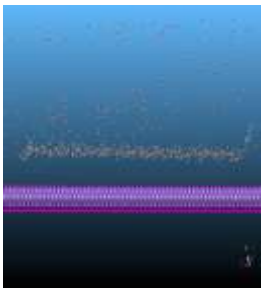	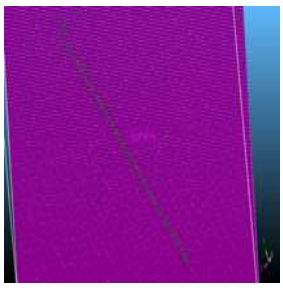

Fig. 12 Mont Carlo simulation of PE-Br-400, PE-Br-1000, PE-Br-4000, and PE-Br-6000.

4. Conclusions.

This study effectively demonstrated the synthesis and assessment of a novel class of environmentally friendly Gemini cationic surfactants derived from polyethylene glycol (PEG) as carbon steel corrosion inhibitors in acidic environments, which are specifically intended to resemble the sever conditions found in oilfield wells and pipelines.

The key conclusions of the study can be summarized as follows:

1-Synthesis and Characterization: The multi-step synthesis strategy successfully produced well-defined Gemini surfactants with varying polyethylene glycol (PEG) chain lengths. The structure and composition of these surfactants were confirmed

through Fourier-transform infrared spectroscopy (FTIR) and proton nuclear magnetic resonance (^1H NMR) spectroscopy. This controlled synthesis approach allows for precise customization of the surfactant properties to achieve optimized performance.

2-Surface Activity: The synthesized surfactants demonstrated significant surface activity, characterized by decreasing critical micelle concentration (CMC) values and increasing surface excess with longer PEG chain lengths. This indicates enhanced adsorption at the air-water interface. Thermodynamic analysis revealed that both micellization and adsorption are spontaneous and exothermic processes, with adsorption being favored at higher temperatures.

3-Corrosion Inhibition: The Gemini surfactants exhibited excellent corrosion inhibition performance for mild carbon steel in a 1N HCl solution, with inhibition efficiency increasing with both surfactant concentration and PEG chain length. This trend was consistently supported by both gravimetric and electrochemical techniques, suggesting the formation of a protective layer on the metal surface through a mixed-type inhibition mechanism.

4-Theoretical and Simulation Insights: Density functional theory (DFT) calculations and molecular dynamics simulations offered profound insights into the adsorption mechanism, demonstrating robust interactions between the cationic head groups and the Fe (110) surface via a combination of electrostatic and hydrogen bonding interactions. Surfactants with longer PEG chains exhibited stronger adsorption, resulting in higher inhibition efficiency.

These findings indicate that PE-Br-6000 exhibits greater efficiency than the other synthesized inhibitors, namely PE-Br-400, PE-Br-1000, and PE-Br-4000. Additionally, these compounds underscore their promising potential as environmentally friendly corrosion inhibitors for oilfield applications. Their unique properties, such as biodegradability and customizable surface activity, make them appealing alternatives to conventional corrosion inhibitors.

Further research is necessary to assess the long-term performance of these surfactants under various oilfield conditions, including temperature fluctuations and the presence of other contaminants. Exploring their synergistic effects with other corrosion inhibitors and optimizing their synthesis for improved yields are also promising areas for future investigation.

5. Conflicts of interest

A conflict of interest has not been declared by the authors.

6. Acknowledgments

I would like to express my heartfelt gratitude to Professor Dr. Madiha Mohammed Hegazy, Professor of Physical Chemistry at the Faculty of Science, Helwan University, for her invaluable scientific guidance and support throughout this research. Additionally, I extend my appreciation to Professor Dr. Emad Abdel Ati Badr from the Egyptian Petroleum Research Institute (EPRI) for his practical assistance, which significantly contributed to the successful completion of this work.

7. References

[1] P. Raffa, A. A. Broekhuis, and F. Picchioni, “Polymeric surfactants for enhanced oil recovery: A review,” *J. Pet. Sci. Eng.*, vol. 145, pp. 723–733, 2016.

[2] S. E. E. Warrag, C. J. Peters, and M. C. Kroon, “Deep eutectic solvents for highly efficient separations in oil and gas industries,” *Curr. Opin. Green Sustain. Chem.*, vol. 5, pp. 55–60, 2017, doi: https://doi.org/10.1016/j.cogsc.2017.03.013.

[3] C. Verma, L. K. M. O. Goni, I. Y. Yaagoob, H. Vashisht, M. A. J. Mazumder, and A. Alfantazi, “Polymeric surfactants as ideal substitutes for sustainable corrosion protection: A perspective on colloidal and interface properties,” *Advances in Colloid and Interface Science*, vol. 318. 2023, doi: 10.1016/j.cis.2023.102966.

[4] P. Hellberg, K. Bergström, and K. Holmberg, “Cleavable surfactants,” *J. Surfactants Deterg.*, vol. 3, no. 1, pp. 81–91, 2000.

[5] A. Lif and M. Hellsten, “Nonionic surfactants containing an amide group,” in *Nonionic Surfactants*, CRC Press, 2017, pp. 177–200.

[6] N. A. Negm, S. A. Ahmed, A. A. Abd-Elaal, and T. Ashraf, “Synthesis and Surface Activity of Nonionic Surfactants Derived from Gallic Acid,” *Arab. J. Sci. Eng.*, vol. 41, no. 1, pp. 67–73, 2016, doi: 10.1007/s13369-014-1488-6.

[7] M. Mobin, S. Zehra, and M. Parveen, “l-Cysteine as corrosion inhibitor for mild steel in 1M HCl and synergistic effect of anionic, cationic and non-ionic surfactants,” *J. Mol. Liq.*, vol. 216, pp. 598–607, 2016, doi: https://doi.org/10.1016/j.molliq.2016.01.087.

[8] M. Stjerndahl, C. G. van Ginkel, and K. Holmberg, “Hydrolysis and biodegradation studies of surface-active esters,” *J. Surfactants Deterg.*, vol. 6, no. 4, pp. 319–324, 2003, doi: https://doi.org/10.1007/s11743-003-0276-z.

[9] A. Pattanaik and R. Venugopal, “Role of Surfactants in Mineral Processing: An Overview,” presented at the International Conference on Mineral Processing, 2019.

[10] N. S. Mousavi, A. Romero-Martínez, and R. Miller, “An empirical model to represent the CMC behavior of aqueous solutions of homologous series of nonionic surfactants, related to its chemical constitution,” *J. Mol. Liq.*, vol. 359, p. 119229, 2022, doi: https://doi.org/10.1016/j.molliq.2022.119229.

[11] A. Fishman, A. Acton, and E. Lee-Ruff, “A Simple Preparation of PEG-Carboxylates by Direct Oxidation,” *Cheminform*, vol. 35, pp. 2309–2312, Aug. 2006, doi: 10.1081/SCC-120038518.

[12] M. A. Migahed, E. G. Zaki, and M. M. Shaban, “Corrosion control in the tubing steel of oil wells during matrix acidizing operations,” *RSC Adv.*, vol. 6, no. 75, pp. 71384–71396, 2016, doi: 10.1039/c6ra12835a.

[13] C. Chen, M. Zhu, M. Li, Y. Fan, and R.-C. Sun, “Epoxidation and etherification of alkaline lignin to prepare water-soluble derivatives and its performance in improvement of enzymatic hydrolysis efficiency,” *Biotechnol. Biofuels*,

vol. 9, no. 1, p. 87, 2016, doi: 10.1186/s13068-016-0499-9.
[14] S. Coupons and F. D. Coupons, “Corrosion Coupons,” vol. 2, no. 32 mm, pp. 1–2.
[15] “VoltaLab Catalog - HACH LANGE - PDF Catalogs | Technical Documentation | Brochure.” [Online]. Available: https://pdf.directindustry.com/pdf/hach-lange/voltalab-catalog/5842-126431.html. [Accessed: 29-Aug-2022].
[16] E. A. Badr, “Inhibition effect of synthesized cationic surfactant on the corrosion of carbon steel in 1 M HCl,” *J. Ind. Eng. Chem.*, vol. 20, no. 5, pp. 3361–3366, 2014.
[17] E. A. Erazua and B. B. Adeleke, “A Computational Study of Quinoline Derivatives as Corrosion Inhibitors for Mild Steel in Acidic Medium,” *J. Appl. Sci. Environ. Manag.*, vol. 23, no. 10, pp. 1819–1824, 2019, doi: 10.4314/jasem.v23i10.8.
[18] A. Jmiai, A. Tara, S. El Issami, M. Hilali, O. Jbara, and L. Bazzi, “A new trend in corrosion protection of copper in acidic medium by using Jujube shell extract as an effective green and environmentally safe corrosion inhibitor: Experimental, quantum chemistry approach and Monte Carlo simulation study,” *J. Mol. Liq.*, vol. 322, no. xxxx, p. 114509, 2021, doi: 10.1016/j.molliq.2020.114509.
[19] M. S. Hussain, M. S. Murtaza, and M. T. Synthesis of Novel Ethoxylated Quaternary Ammonium Gemini Surfactants for Enhanced Oil Recovery Application, "Energies," vol. 12, no. 9, 2019, doi: 10.3390/en12091731.
[20] K. Shameli *et al.*, “Synthesis and Characterization of Polyethylene Glycol Mediated Silver Nanoparticles by the Green Method,” *Int. J. Mol. Sci.*, vol. 13, no. 6, pp. 6639–6650, Dec. 2012, doi: 10.3390/ijms13066639.
[21] E. S. Material, M. Chemistry, and T. R. Society, “H NMR spectra of PEG-R H NMR of synthesized PEG-S,” vol. 63, 2013.
[22] O. Hari and S. K. Upadhyay, “Rhamnolipid–metal ions (CrVI and PbII) complexes: Spectrophotometric, conductometric, and surface tension measurement studies,” *J. Surfactants Deterg.*, vol. 24, no. 2, pp. 281–288, 2021, doi: 10.1002/jsde.12481.
[23] N. A. Negm and A. S. Mohamed, “Surface and thermodynamic properties of diquaternary bola-form amphiphiles containing an aromatic spacer,” *J. Surfactants Deterg.*, vol. 7, no. 1, pp. 23–30, 2004, doi: https://doi.org/10.1007/s11743-004-0284-z.
[24] N. A. Negm, M. A. El Hashash, A. Abd-Elaal, S. M. Tawfik, and A. Gharieb, “Amide type nonionic surfactants: Synthesis and corrosion inhibition evaluation against carbon steel corrosion in acidic medium,” *J. Mol. Liq.*, vol. 256, pp. 574–580, 2018.
[25] J. C. Therm, B. Kumar, D. Tikariha, K. K. Ghosh, N. Barbero, and P. Quagliotto, “Effect of polymers and temperature on critical micelle concentration of some gemini and monomeric surfactants,” *J. Chem. Thermodyn.*, vol. 62, pp. 178–185, 2013, doi: 10.1016/j.jct.2013.03.006.
[26] I. Aiad, M. Abo Riya, S. M. Tawfik, and M. A. Abousehly, “Synthesis, surface properties and biological activity of N,N,N-tris(hydroxymethyl)-2-oxo-2-(2-(2-(alkanoyloxy) ethoxy)ethoxy) ethanaminium chloride surfactants,” *Egypt. J. Pet.*, vol. 25, no. 3, pp. 299–307, 2016, doi: https://doi.org/10.1016/j.ejpe.2015.07.020.
[27] V. B. Wagle, P. S. Kothari, and V. G. Gaikar, “Effect of temperature on aggregation behavior of aqueous solutions of sodium cumene sulfonate,” *J. Mol. Liq.*, vol. 133, no. 1, pp. 68–76, 2007, doi: https://doi.org/10.1016/j.molliq.2006.07.006.
[28] D. J. Shaw, *Introduction to colloid and surface chemistry*. Butterworths, 1980.
[29] H. Kumar, J. Kaur, and P. Awasthi, “Investigation of aggregation and surface active properties of cationic Gemini surfactants in the presence of antidepressant drug,” *Colloids Surfaces A Physicochem. Eng. Asp.*, vol. 641, p. 128539, 2022, doi: https://doi.org/10.1016/j.colsurfa.2022.128539.
[30] H. Kumar and R. Kaur, “Studies on thermodynamics of micellization of imidazolium-based surface-active ionic liquid [C15mim][Br] in aqueous media: Effect of D(+)-Xylose and D(+)-Glucose,” *J. Mol. Liq.*, vol. 344, p. 117645, 2021, doi: https://doi.org/10.1016/j.molliq.2021.117645.
[31] N. A. Negm, A. F. M. El Farargy, D. E. Mohammed, and H. N. Mohamad, “Environmentally friendly nonionic surfactants derived from tannic acid: synthesis, characterization and surface activity,” *J. Surfactants Deterg.*, vol. 15, no. 4, pp. 433–443, 2012.
[32] A. M. Al-Sabagh, N. M. Nasser, O. E. El-Azabawy, and A. E. El-Tabey, “Corrosion inhibition behavior of new synthesized nonionic surfactants based on amino acid on carbon steel in acid media,” *J. Mol. Liq.*, vol. 219, pp. 1078–1088, 2016, doi: 10.1016/j.molliq.2016.03.048.
[33] M. M. Hegazy, E. M. Khalil, E. Badr, and M. A. F. Mansour, “Amino pyridine derivatives as new corrosion inhibitors for protection cabling metal of crude oil well during acidizing,” *Egypt. J. Pet.*, vol. 32, no. 4, pp. 8–20, 2023.
[34] G. Gece, “The use of quantum chemical methods in corrosion inhibitor studies,” *Corros. Sci.*, vol. 50, no. 11, pp. 2981–2992, 2008.
[35] G. Gao and C. Liang, “Electrochemical and DFT studies of β-amino-alcohols as corrosion inhibitors for brass,” *Electrochim. Acta*, vol. 52, no. 13, pp. 4554–4559, 2007.
[36] J. Zhang, J. Liu, W. Yu, Y. Yan, L. You, and L. Liu, “Molecular modeling of the inhibition mechanism of 1-(2-aminoethyl)-2-alkyl-imidazoline,” *Corros. Sci.*, vol. 52, no. 6, pp. 2059–2065, 2010.
[37] M. Chafiq *et al.*, “Unveiled understanding on corrosion inhibition mechanisms of hydrazone derivatives based on naproxen for mild steel in HCl: A joint experimental/theoretical study,” *J. Mol. Liq.*, vol. 320, 2020, doi: 10.1016/j.molliq.2020.114442.
[38] A. Hossam *et al.*, “Molecular dynamic simulation studies and surface characterization of carbon steel corrosion with changing green inhibitors concentrations and temperatures,” pp. 2492–2519, 2022.